Acta Geochim (2026) 45:384–401
https://doi.org/10.1007/s11631-025-00778-7

ORIGINAL ARTICLE

Mineralogical and geochemical features of Sirginil phyllite group from Penjween area, Iraqi Kurdistan region: Implications for provenance and source-area weathering

Tola A. Mirza[1] · Stavros P. Kalaitzidis[2] · Shahra O. Abdalla[3] · Sofia Tsiotou[2]

Received: 10 November 2024 / Revised: 21 March 2025 / Accepted: 23 March 2025 / Published online: 24 April 2025
© The Author(s), under exclusive licence to Science Press and Institute of Geochemistry, CAS and Springer-Verlag GmbH Germany, part of Springer Nature 2025

Abstract The Sirginil Phyllite Group being outcropping in Penjween area is investigated to determine the provenance and weathering level of the source area. Petrographic investigation of the phyllites shows that they are almost homogeneous in composition and highly crenulated. The most prominent features are kink band structures and network fabrics, consisting mainly of fine-grained mineral assemblages of chlorite, muscovite, quartz, and plagioclase feldspar. The geochemical data indicate that the phyllite rocks represent precursors of shales and greywackes as their protolith, having undergone an intensive degree of chemical weathering without sorting. Additionally, the presence of graphite, as an indication of organic matter, points to quick transport and burial of the protolith sedimentary rocks, which originated from a unique source area. The average values of the chemical alteration index and chemical weathering index indicate that a high degree of weathering of the source materials occurred in a humid environment. The Th/U ratio, as well as the concentrations of Th and U, indicates a sedimentary origin and oxidizing conditions during sedimentation of the protolith rocks. The REE pattern coupled with prominent negative Eu anomaly and low Th/Sc ratios, as well as the plots of La/Sc versus Th/Sc, La/Yb versus La/Ce, and Th/Yb versus Ta/Yb, indicates a continental margin as the paleoenvironment of the sedimentary protolith. The Th/Sc ratios for the studied samples denote origin from a predominantly felsic igneous source, while the median Zr/Sc ratio indicates only a minor degree of sorting and zircon addition in all the studied samples.

Keywords Sirginil phyllites group · Graphite · Allanite · REE pattern · Palaeoenvironment

1 Introduction

The phyllites of the Sirginil Group in Mlay Lexaugira area are situated in NE Iraq, close to the Iranian borders, about 10 km northeast of Penjween Town, Sulaimani Governorate (Figs. 1A, B and 2 A). The rock formations of the studied area belong to the Qandil Thrust Block, developed along shear zones in the northwestern part of the Zagros Orogeny, endowed with a wide variety of mineral resources, some of which occur in considerable quantities and with exploitable qualities (Mirza et al. 2017, 2021).

The Zagros Orogeny Belt resulted from the Late Cretaceous and Cenozoic convergence of the Iranian terranes and the Arabian Plate when the intervening Neo-Tethys Ocean went through a succession of subduction, obduction, and collision stages (Alavi 1994, Sharland et al. 2001, Agard et al. 2005, Al-Qayim et al. 2012, Ismail et al. 2017, Mustafa

Supplementary Information The online version contains supplementary material available at https://doi.org/10.1007/s11631-025-00778-7.

✉ Tola A. Mirza
tola.merza@univsul.edu.iq

Stavros P. Kalaitzidis
skalait@upatras.gr

Shahra O. Abdalla
shahraosman@gmail.com; shahra.othman@uhd.edu.iq

Sofia Tsiotou
sofia.tsiotou0@gmail.com

[1] Earth Sciences and Petroleum, University of Sulaimani, Sulaimani, Kurdistan Region, Iraq

[2] Department of Geology, University of Patras, 26504 Rio-Patras, Greece

[3] Development Center for Research and Training, University of Human Development, Sulaymaniyah, Kurdistan Region, Iraq

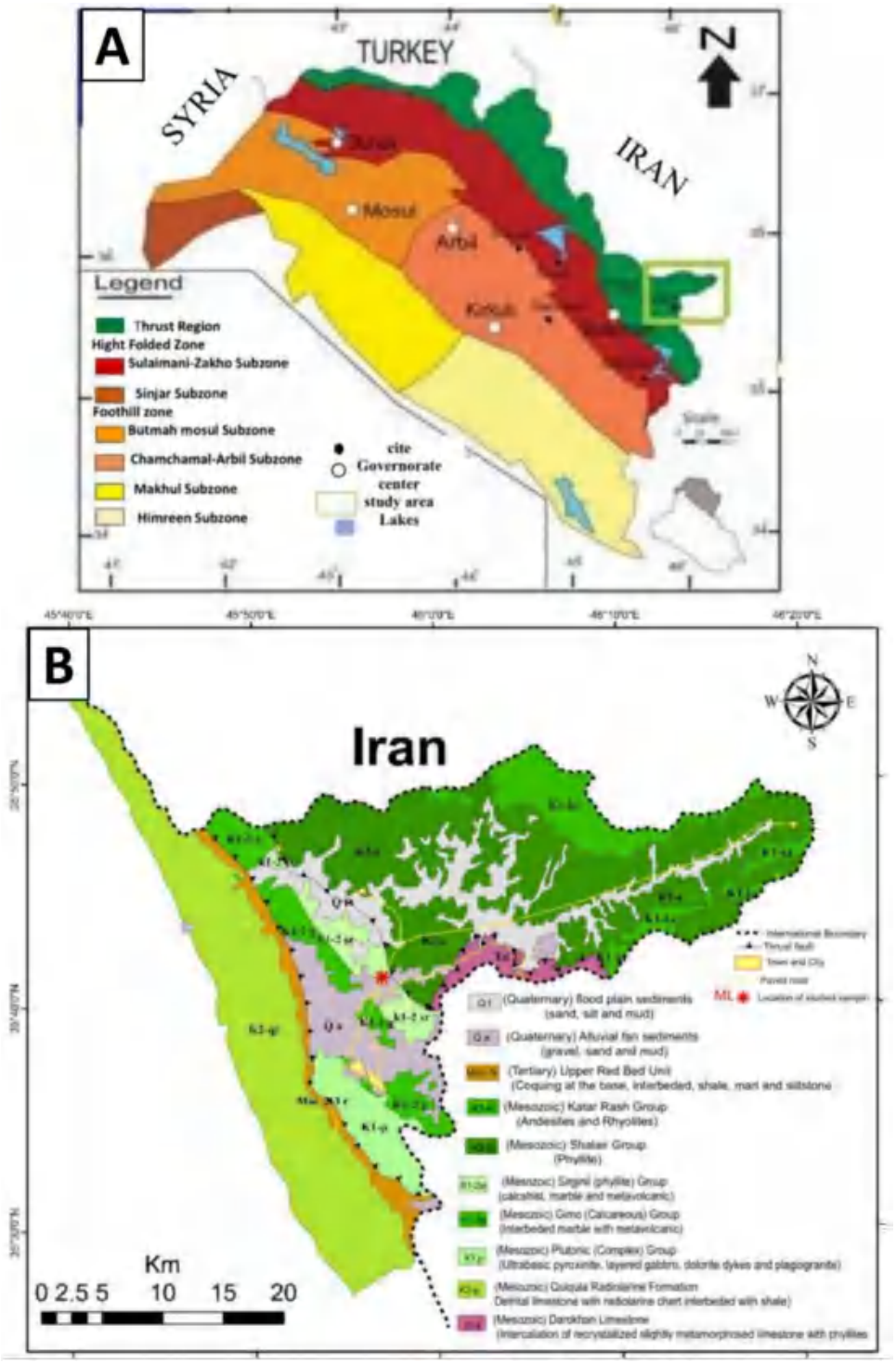

Fig. 1 **A** Tectonic subdivision of NE Iraq after Al-Kadhimi (1996); **B** geological map of the southern part of the Zagros Suture Zone, located in NE Iraq, displaying the studied area after Ma'ala (2008)

et al. 2023). The studied area is structured of alternating successions of phyllites and massive beds of marble. They are cropped out as disconnected beds, sometimes brecciated and usually fractured, with widespread quartz veins and veinlets, which cut across both the phyllites and marbles (Fig. 2B). The phyllite of Mlay Lexaugira ranges in width from 10 to 50 m and extends to >500 m. This phyllite is cross-cut by quartz veins; the forms of these quartz veins are variegated depending on the basic rock fissuring, content, and origin conditions. The veins range in length from a few centimeters to several meters with varying thickness and granularity. The phyllite is composed mainly of low metamorphic rocks, which constitute much of the Sirginil Group. Phyllites in general are foliated, fine-grained rocks, originating from

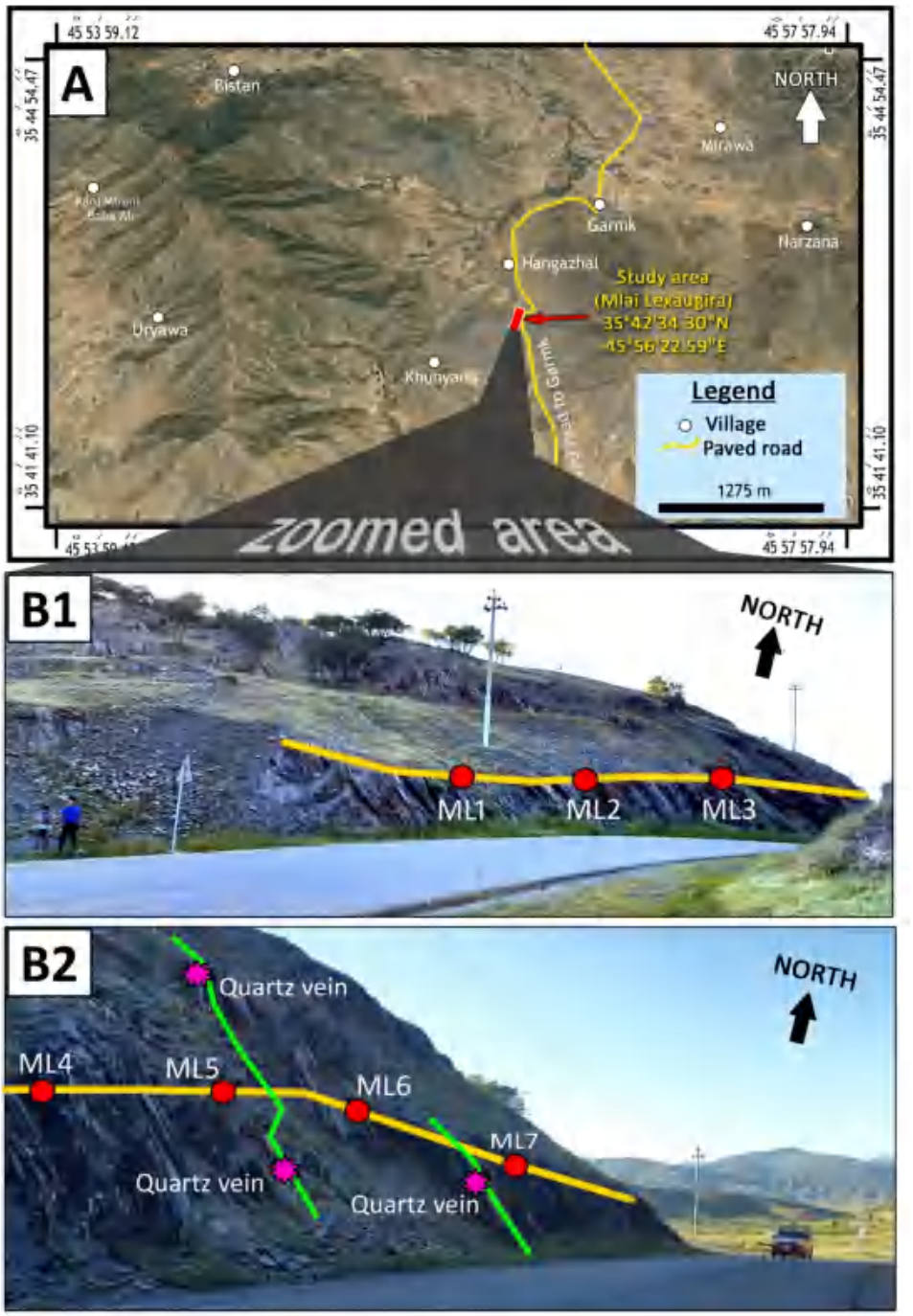

Fig. 2 Satellite image of the studied area (Google Earth maps) and details of the sampling scheme (ML 1–7: samples)

low-grade regional metamorphism of pelites, and are composed mainly of quartz, albite, and phyllosilicates, such as muscovite and chlorite (Silwal et al. 2024).

Using elemental geochemical features to determine the paleo-depositional environment of the basin is very important for determining the tectonic setting (Rana et al. 2023). Determination of the composition of rocks in Mlay Lexaugira area using x-ray fluorescence spectrometry, inductively coupled mass spectrometry (ICP-MS), scanning electron microscopy (SEM) and thin section petrography were necessary to obtain more comprehensive geological information on the phyllites of the studied area. By combining the geological information with a detailed chemical classification of the rocks in the area, using dominant mineralogical compositions, prediction of the petrogenesis and protoliths of the rocks in selected studied area could be made. In this paper, the authors discuss the mineralogical, petrographic, and geochemical characteristics of phyllites to understand their provenance, tectonic setting, and the paleoenvironment of depositions. Therefore, a variety of methods were used to

study the phyllite rocks in the selected area, such as petrographic study and geochemical analysis (i.e., determination of major, minor, and rare earth element concentrations) in bulk rock samples. Additionally, the chemical compositions of phase minerals were determined.

2 Geological setting

Mlay Lexaugira phyllites are a part of the Sirginil phyllite Group. This complex geological area is situated at the northeastern edge of the Iraqi Zagros suture zone (IZSZ) (Fig. 1A). The IZSZ represents a part of the larger Zagros Suture, which belongs to the Alpine-Himalayan Orogenic Belt that extends northwestward to Turkey and southeastward to Iran. The lithology in the studied area belongs to the Qandil metamorphic series (QMS) of the Penjween-Walash Zone, which develops in the Iraqi Zagros Suture Zone, based on the tectonic subdivision of Iraq by Buday (1980) (Fig. 1A). This series represents low-metamorphosed limestones and schists, building to the frontier range of eastern Iraq, and structurally overlays the Walash and Naopurdan Series. The Penjween-Walash Zone is a unit of the Central Neo-Tethys, which was thrust over the Arabian Plate by an obduction and collision process during the Miocene-Pliocene epoch (Jassim and Goff 2006, Mustafa et al. 2023, Qaradaghy and Mirza 2023). It forms a continuous belt along the Iraq-Iran borders, being constructed by metamorphosed sedimentary and volcanic rocks of the Cretaceous and unmetamorphosed Palaeogene forearc and volcanic-arc rocks, which formed during the final closure of the Neo-Tethys (Jassim and Goff 2006). Tectonically, Penjween-Walash Zone is overlain and thrust over the Qulqula-Khwakurk Zone or the Balambo-Tanjero Zone, whereas the Shalair Zone, which structurally forms the highest thrust sheet in Iraq, is thrust over the Penjween-Walash Zone (Jassim and Goff 2006). The Qandil Metamorphic Series is subdivided into the Mawat, Gimo, and Sirginil Groups, from the youngest to the oldest, respectively.

The investigation area is named Mlay Lexaugira (local name), located 10 km far from Penjween town to the north on the main paved road in Penjween-Garmk (coordinates: 35°42′34.30″ N, 45°56′22.59″ E (Figs. 1 A, B and 2A). The studied area represents a part of Sirginil Group (Fig. 1B). The Sirginil Group is composed of metamorphosed limestones, calcphyllites, phyllites and sparse conglomerates, without any volcanic admixture. The contact of the Sirginil Group with the overlain sedimentary unit is erosional, while the contact between Gimo and Sirginil Groups is of tectonic nature (Mirza et al. 2017). The outcropped phyllite beds in the studied area are inclined NE; the phyllites are dark brown in color, strongly foliated, and often fractured with widespread cross-cutting of quartz veins and veinlets that cross-cut the phyllite in the form of an open space-filling texture (Fig. 2 B2) (Mirza et al. 2022).

3 Materials and methods

Seven representative fresh rock samples were selected from 20 samples collected during the field work for laboratory analysis. Samples were obtained from an outcrop covering all observable variations. Thin sections were prepared for petrographic study under transmitted light at the Department of Earth Sciences and Petroleum, University of Sulaimani.

Mineral assemblages in the phyllites were determined in powdered (−50 μm) samples by using a a Bruker D8 X-ray Diffractometer equipped with a Lynx-Eye® detector. EVA and Topas softwares were used to determine the qualitative and quantitative features of the mineral phases, respectively, at the facilities of the Department of Geology, University of Patras. Polished blocks from rock slabs were prepared and examined using a LEICA DMRX coal petrography microscope to study the texture and microstructural characteristics of the phyllites and the identified graphite flakes.

X-ray fluorescence (XRF) analysis for major and minor elements was performed using a RIGAKU ZSX PRIMUS II spectrometer, equipped with a Rh-anode. Loss on ignition (LOI) values were determined by combusting 1 g at 950 ℃ for 2 h (Heiri et al. 2001) using a Selecta muffle furnace at the facilities of the Department of Geology, University of Patras.

Additionally, chemical compositions of minerals in gold-coated polished blocks of samples ML1 and ML3 were determined using JEOL JSM 6300 fitted with an EDS X-ray analyzer. SEM and XRF analyses were performed at the facilities of the Laboratory of Electron Microscopy and Microanalysis of the University of Patras, Greece. Finally, the rare earth element (REE) content was determined by using sodium peroxide fusion/combined ICP-AES and ICP-MS in the SGS laboratory in Canada.

4 Results and discussions

4.1 Petrographic and mineralogical features

The studied phyllites display well-developed schistosity and planar to crumple foliation, representing fine-grained and thinly banded, regionally metamorphosed foliated pellitic rocks.

The pressure causes development of the foliation, where mineral grains are well arranged into alignment and layers (Awadh and Kettanah 2008). Hence, the presence of schistosity and crenulation cleavage indicates at least two phases of deformations. They are characterized by silky luster,

displaying shades of brown and yellow colors, with the dark color being related to higher chlorite content (Figs. 3 and 5). The metamorphic grain size of phyllites evidently copies the former inherited sedimentary grain size (Figs. 3 and 5). According to the grain-size scale (Wentworth 1922), the studied samples range from silt (siltstone, clay, mud) to very fine-grained sand (grain size < 0.0625 mm); hence, the studied phyllite rocks are fine schistose and often display dark colors caused by the high chlorite content and frequently wide-spread organic pigments (Figs. 3 and 5). X-ray diffraction indicates that quartz, muscovite, chlorite, and albite are the major constituents of phyllites, while siderite, orthoclase, and graphite occur as accessory minerals (Table 1, Fig. 4). The amount of quartz ranges from 34 to 44 wt% in the most studied phyllites, while albite varies from 5 to almost 20 wt%. Samples show variable concentrations of clinochlore and muscovite, varying from <10 to ~24 wt% and from 12 to 20 wt%, respectively. The clinochlore to muscovite ratio ranges from 0.0 to 1.3, with muscovite being the predominant phyllosilicate in most samples (Table 1). Sample ML5 is enriched in K-feldspars (~16 wt%) and is relatively depleted in albite (10 wt%). The observed differences in the mineral composition of phyllite samples probably reflect the variability of the protolith. The argillaceous protolith turned into muscovite-chlorite-rich assemblages, whereas the higher silt fraction reflects a psammitic protolith.

Under the microscope, the phyllites are almost similar in composition and highly crenulated, showing a kink band structure and network fabrics. They are fine-grained foliated rocks occasionally showing segregation layering. The main identifiable minerals (< 0.1 mm) include quartz, plagioclase feldspar, chlorite, muscovite, and dark chlorite, whereas hematite, allanite, rhodonite, and graphite are present as very minor constituents (Figs. 5 and 6). Finally, calcite occurs as intra-foliated grains, as well as within veinlets cross-cutting the phyllite. Elongated, lenticular quartz grains (clasts) are up to ~25 mm long and ~10 mm thick. They are aligned parallel to the foliation (Fig. 5A) and often have an augen structure. Individual augens, usually present

Fig. 3 **A–C** Field views of the phyllites showing thin banding, schistosity, minor folds, and crenulation cleavage

Table 1 XRD mineralogical composition of the studied phyllites and quartz veins (in % of the crystalline phases)

Samples	Ml_1	ML_2	ML-3	ML_4	ML_5	ML_6	ML_7
Quartz	41	42	35	34	35	44	41
Albite	14	20	5	12	10	14	10
Muscovite	18	11	17	12	20	20	20
Clinochlore	24	21		8	18	19	20
Chamosite			26	30			
Orthoclase			10				8
Microcline					16		
Siderite			2				
Calcite			4				
Graphite	3	6	1	4	1	3	1
Total	100	100	100	100	100	100	100
Clinochlore /muscovite	1.33	1.91	0.00	0.67	0.90	0.95	1.00

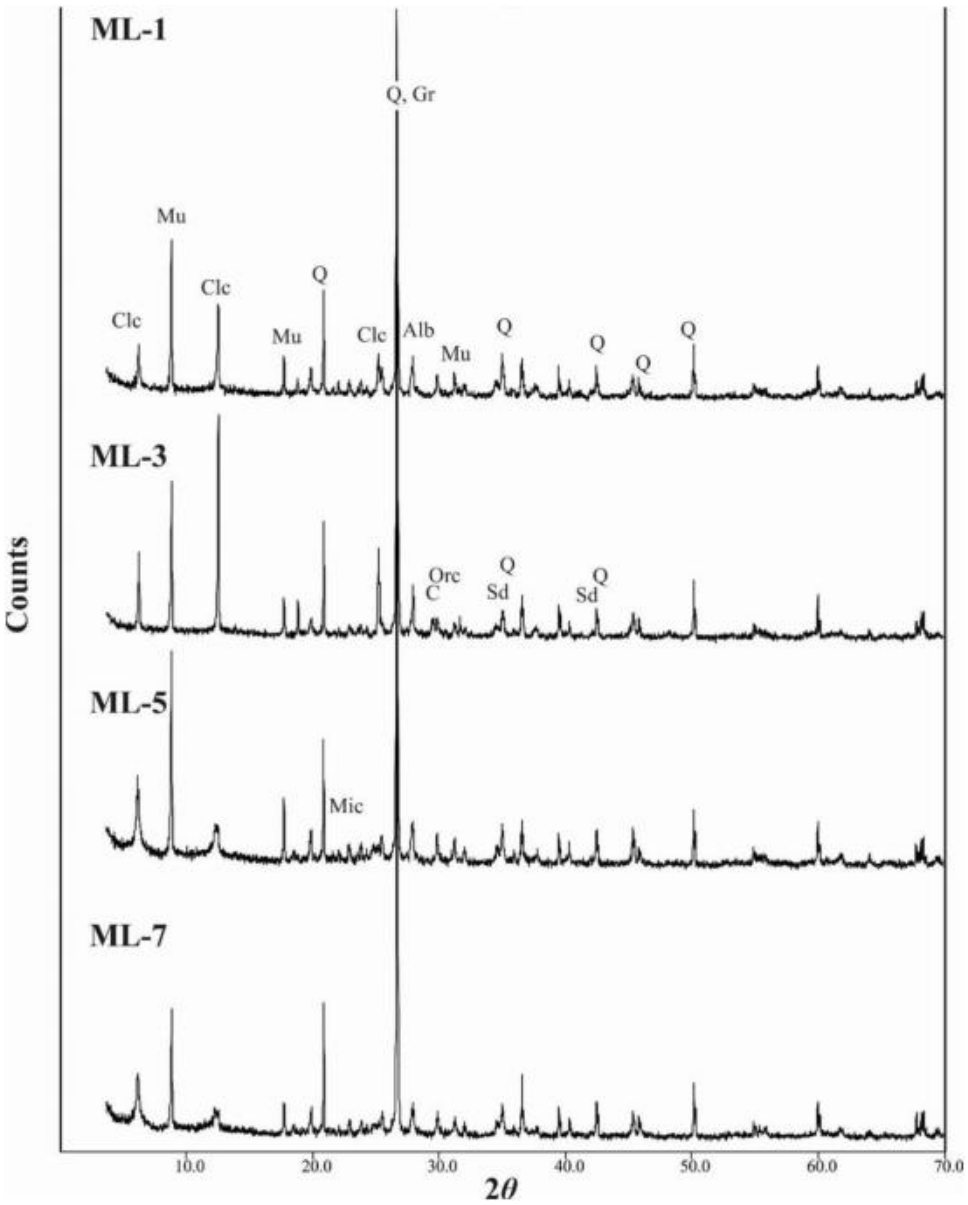

Fig. 4 X-ray diffractograms of the studied phyllite samples

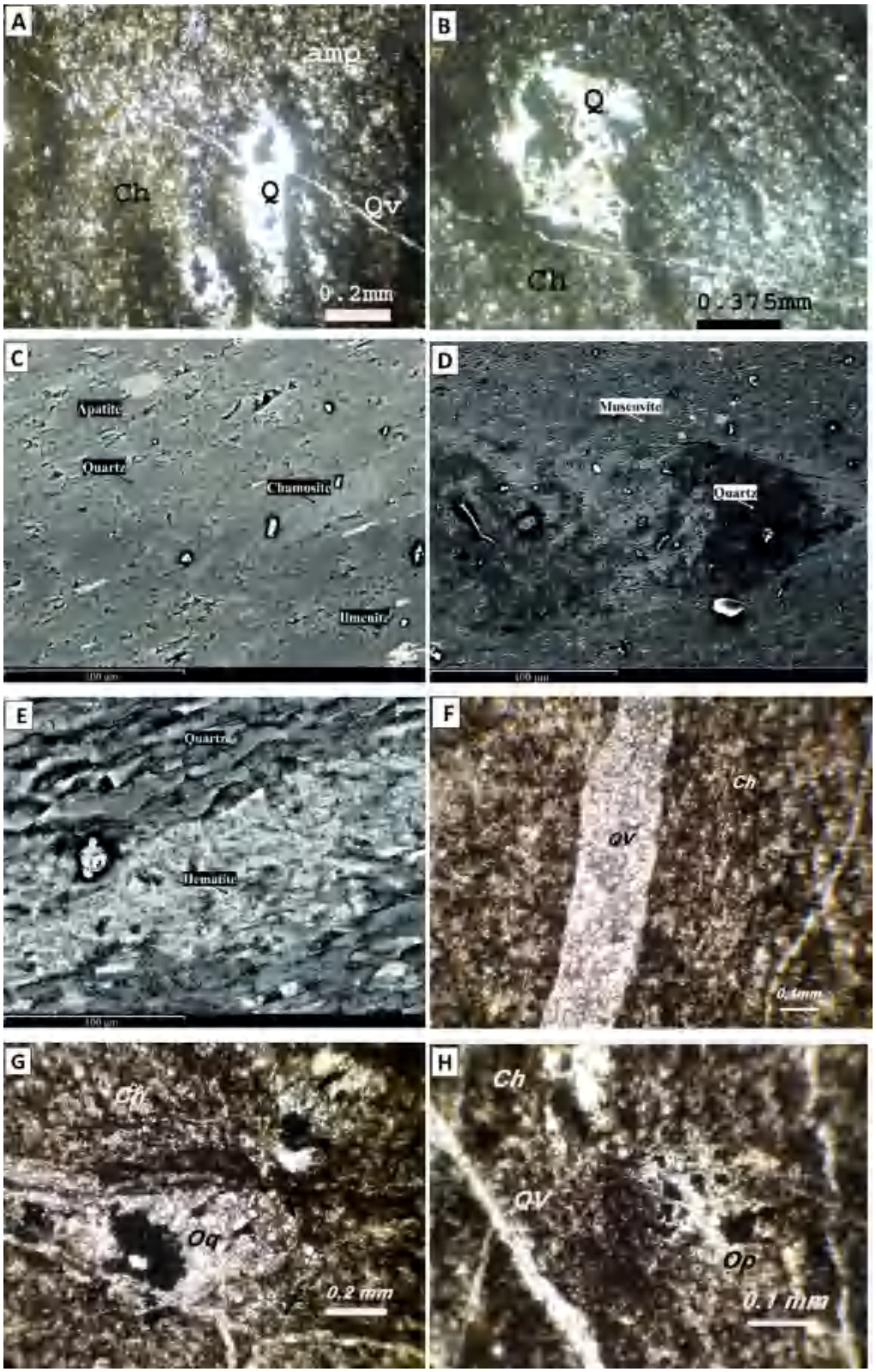

Fig. 5 **A** Photomicrograph of phyllite displaying fine grain texture and containing elongated quartz aggregated lensoid grains and quartz veinlets; **B** photomicrograph of phyllite containing porphyroblasts of quartz and pressure shadows of chlorite, with quartz veinlets transecting the rock matrix; **C**, **D** and **E** SEM images of the phyllite mineral constituent; **F** thin cross-cutting veinlet of crystalline quartz within a phyllite sample; **F** thin cross-cutting veinlet of crystalline quartz within a sample of phyllite; **G** opaque mineral representing hematite; **H** anhedral fine grain opaque mineral (Q: quartz; Qv: quarz vein; Ch: chlorite; amp: amphibole, Oq: opaque mineral mainly represents hematite, siderite, and illmenite

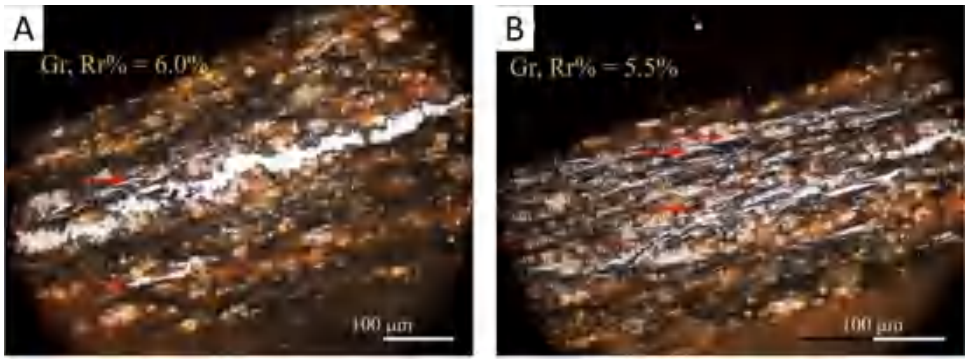

Fig. 6 Photomicographs of a polished block ofphyllite taken under white reflected light, oil immersion, X500, displaying graphite layers with the respective reflectance values

within the fine-grained matrix, are formed by plagioclase and quartz, representing former clasts. Albite grains are of similar size, but unlike quartz they are angular and apparently less deformed. Muscovite and chlorite are intimately intergrown (Fig. 5B), although in some cases chlorite overgrows muscovite. There are two generations of chlorite: the fine-grained one in the phyllite matrix and coarse aggregates within quartz veins that cross-cut phyllite (Fig. 5 A, B). The latter generation shows anomalous indigo blue interference colors under the polarizing microscope. Ilmenite and hematite are ubiquitous accessory minerals; they are often intergrown with quartz and display features indicative of partial dissolution; for instance, their grain boundaries are embayed and irregular (Fig. 5C–G). Allanite, apatite, hematite, siderite, ilmenite and rhodonite are accessory minerals.

The textures and microstructures of the studied phyllites point to a very high degree of orientation, with elongation of quartz, either as grains or narrow aggregated lenses and stringers, and with chlorite in parallel flakes and pods (Fig. 5F and G). Iron oxide minerals appear in rounded and dusty clouds or as finely disseminated grains. Some phyllites contain porphyroblasts of quartz and pressure shadows of chlorite (Fig. 5A and B). Moreover, quartz veins and veinlets often transect the rock mass (Fig. 5E and F). Additionally, laminae of very fine-grained graphite alternate with granular quartz, muscovite, and chlorite (Fig. 6A and B). The mean random reflectance values (Rr) of the graphite range between 5.5% and 6%.

4.2 Whole rock chemical composition

4.2.1 Major element composition

All investigated samples have similar bulk chemical compositions, displaying high SiO_2 concentrations (56.56–62.26 wt%), because of the high quartz content (Table S1). The silica content is inversely correlated with the concentration of aluminum (Fig. 7), with a negligible variation in the SiO_2/Al_2O_3 ratio (Table S1). The average concentrations of K_2O (3.89%) are generally higher than those of Na_2O (0.86%). The contents of Fe_2O_3 (6.31%–7.76%), MgO (1.56%–2.56%), CaO (0.17%–2.16%), and TiO_2 (0.76%–0.96%) are relatively low indicating a low abundance of mafic minerals. The geochemical approach to defining the nature of the source area and the tectonic setting of the depositional basin is applied by using discrimination plots based on major element compositions of the phyllites. The diagram of average values of SiO_2 wt% (58.9 wt%) and Al_2O_3 (19.06 wt%) indicates that Sirginil phyllites fall into the meta-pelite group (Fig. 7), with protolith suffering intensive weathering without sorting. The presence of graphite (Fig. 6) indicates relatively quick transport and burial of the protolith from the source area, evidenced by the organic precursors, which are not totally weathered and oxidized as well. It suggests that samples of the studied area have a similar composition to the parental rocks. The geochemical discrimination diagram by Herron (1988) indicates that the studied phyllites are ascertained in a relatively narrow field corresponding to greywackes and shales (Fig. 8). Relatively high concentrations of TiO_2, compared to low concentrations of this element in chlorite and muscovite suggest accessory ilmenite as a major carrier of TiO_2, as detected using SEM (Fig. 5C).

Increased concentrations of CaO in sample ML3 (Table S1) coincides with the observation of intra-foliated calcite grains (Table 1) and accessory apatite (Fig. 5C). The concentration of K_2O predominates over Na_2O, ranging between 3.1% to 4.25% and 0.58% to 1.44%, respectively. The ratio of Na_2O/K_2O varies between 0.14 and 0.46, corresponding to the proportions between albite and muscovite or between orthoclase and microcline. Cox et al. (1995) used the K_2O/Al_2O_3 ratio as an indicator of the original composition of ancient sediments and defined this ratio for clay minerals and feldspars as 0.0 to 0.3 and 0.3 to 0.9, respectively. The K_2O/Al_2O_3 ratios of the studied samples range from 0.17 to 0.22 (Table S1), suggesting that muscovite is the most abundant phyllosilicate of the studied phyllites.

All samples are ferruginous and are enriched in Fe_2O_3 relative to MgO, as indicated by the high $Fe_2O_3/(Fe_2O_3 + MgO)$ ratio values, ranging between 0.75 and

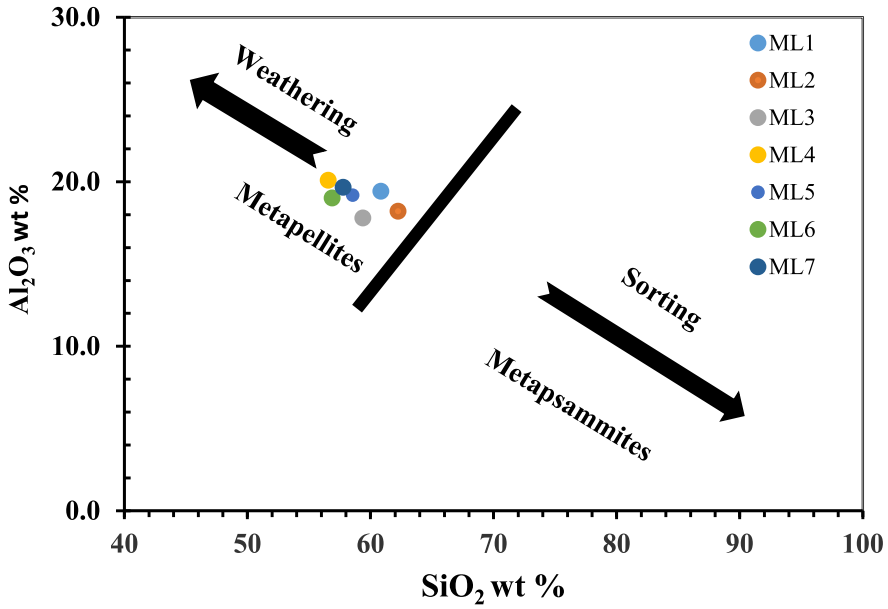

Fig. 7 Plots of Al_2O_3 versus SiO_2 for the Mlay Lexaugira phyllite rock fields regarding lithologies and processes after Méres (2005)

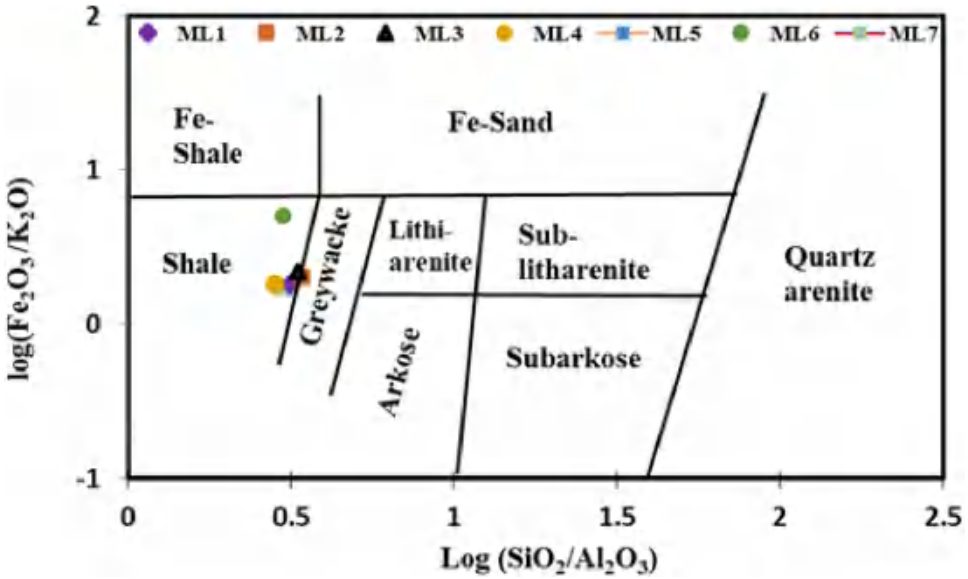

Fig. 8 Geochemical classification of the Mlay Lexaugira phyllites after Herron (1988)

0.83, with an average of 0.78 (Table S1). The loss of ignition (LOI) values reflect the relatively high concentration of water in the phyllosilicates and the contribution of graphite. Overall, the chemical composition of the argillaceous phyllites from the Sirginil Group in Mlay Lexaugira area resembles the average chemical composition of pelagic pelites. The notable differences include a lower SiO_2/Al_2O_3 ratio and a higher Na_2O/K_2O ratio in the latter. The much lower content of water in phyllite samples compared to pelites can simply be explained by water loss during pelites metamorphism. A metasedimentary origin of studied samples is confirmed by the diagram of K_2O/Al_2O_3 against Na_2O/Al_2O_3, since all samples plot in the meta-sedimentary origin field (Fig. 9).

4.2.2 Trace elements

The trace element concentrations in the studied phyllites compared to the average estimates of the Early Proterozoic crust (Condie 1993) show that all samples have limited amounts of both large ion lithophile elements (LILE) and high-field-strength elements (HFS) but are enriched in first series transition metals (Fig. 10). The concentrations of Ni and Cr in siliciclastic sediments are considered a useful

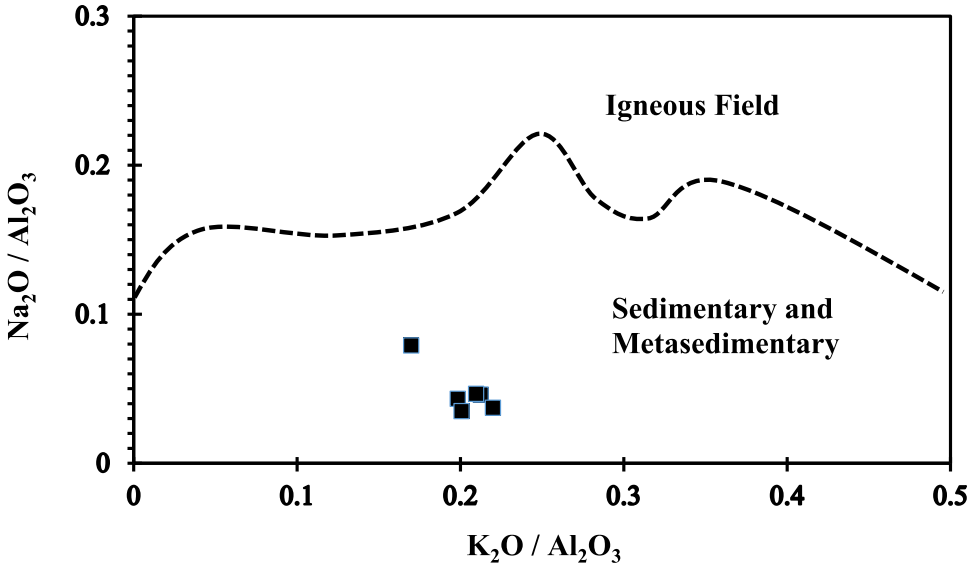

Fig. 9 Alkali-Silica diagram of the Mlay Lexaugira phyllites, modified after MacDonald and Katsura (1964)

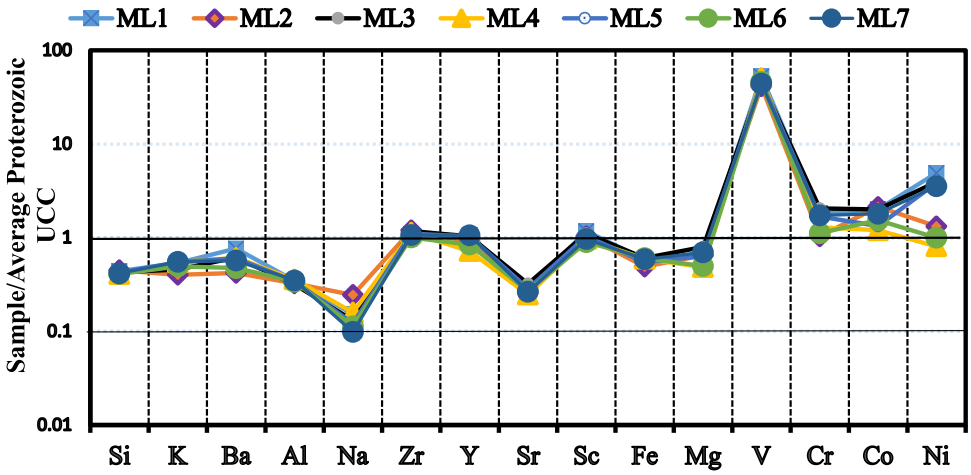

Fig. 10 Upper crust normalized patterns for the studied samples; normalized values of early Proterozoic crust from Condie (1993)

indicator in provenance studies (Aliyari et al. 2014). Average Ni and Cr concentrations and average Cr/Ni ratios of the Sirginil phyllites are 85.7 ppm, 90.43 ppm, and 1.45, respectively (Table S1), and for earlyProterozoic upper crust are 31 ppm, 59 ppm and 1.90, respectively (Condie 1993). Wrafter' and Graham (1989) and Kwankam et al. (2023) proposed that a low concentration of Cr indicates a felsic provenance. Bock et al. (1998) designated enriched ferromagnesian elements (e.g., Fe, Cr, Ni) to the contribution of mafic and ultramafic igneous rocks. Besides, elevated concentrations of these elements in the sediments and sedimentary rocks may indicate addition of components derived from mafic lithologies.

High Cr and Ni concentrations with low Cr/Ni (between 0.7 and 3.04) were further suggested to be indicative of ultramafic rocks in the source area of shales by Garver et al. (1996) and Bokanda et al. (2021). The above presented Cr, Ni, and Cr/Ni data therefore suggest the influence of mafic and ultramafic lithologies during sedimentation of the protolith of the metamorphosed sedimentary rocks for Sirginil phyllites. Variable contents of Th and U in metamorphosed sedimentary rocks indicate variable oxidation-reduction conditions during their sedimentation (Cambel and Khun 1983, 1985, Cambel and Planderová 1985). Relatively high values of the Th/U ratio (>1) at higher contents of Th (>5 ppm) and lower contents of U (<5 ppm) in metamorphosed sedimentary rocks indicate oxidizing conditions during sedimentation. The Th/U ratio and thorium range also indicate a common source area and the same parental rocks. This is also confirmed by the similar range of Th/U ratios in metamorphosed sedimentary rocks and E-MORB-type metabasalts, while the low contents of Th (<5 ppm) and high contents of U (U > 5 ppm) in metamorphosed sedimentary rocks indicate reducing conditions during sedimentation. Similarly, the range of Th/U and the values of Th

(<5 ppm) and U (>5 ppm), as recorded in N-MORB-type metabasalts, indicate synchronous basic volcanism during sedimentation of the protolith of metamorphosed sedimentary rocks (Ivan et al. 2001). Additionally, according to Wignall and Twitchett (1996), the Th/U ratio in the anoxic environments is <2, whereas it is >2 (up to 7) in rocks deposited under oxic conditions.

The Th/U (4.4–8.02) and range values of Th and U content of the studied samples, Th (10–20 ppm) and U (1.99–2.93 ppm) (Table S1), indicate a sedimentary rock origin and oxidizing conditions during sedimentation. The La/Sc ratio in very fine-grained siliciclastic sediments resembles the average La/Sc ratio in the source area of sedimentary rocks (Cullers 1995). The average La/Sc, and Th/Sc in the studied samples are >1.6 and <1.0, respectively, indicating deposition in sedimentary rocks of the continental margin environment (Fig. 11A). The studied phyllite samples are well discriminated by values of La/Yb against La/Ce ratios (Fig. 11B). The high value of La/Yb (6.79–11.56) indicates higher crustal fractionation of the parental rocks in the source area. Additionally, the range of the La/Ce ratio in the studied samples indicates Ce enrichment in the Sirginil phyllite because of the interaction of hydrothermal fluids during metamorphism. This is further supported by the presence of allanite within the quartz veins in the studied samples. The high values of Th/Yb (>2.8) and Ta/Yb (>0.4) ratios also indicate sedimentation at the continental margins (Fig. 11C, Table S1).

4.2.3 Rare earth element geochemistry

The REE data of the phyllite samples were normalized using chondrite values from Palme (1988). The chondrite-normalized REE signatures of the Sirginil phyllites are similar to the North American shale composition (NASC), indicating a possible sedimentary pre-metamorphic protholith (Fig. 12) (Gromet et al. 1984; Mclennan 2018). In general, the chondrite normalized REE pattern for the studied samples shows an enrichment of light REE (LREE) and flat heavy REE (HREE), with a negative Eu anomaly. The most important characteristics include the Eu negative anomaly, with Eu/Eu* varying from 0.54 to 0.72. The negative Eu anomaly probably is caused by fractionation of substantial plagioclase, which in turn confirms the presence of plagioclases in the protolith. The (La/Yb)n ratios range between 10.1 and 10.4, distributed with approximately uniform patterns, horizontal HREE patterns, and moderately enriched LREE with (Gd/Yb)n between 1.29 and 1.57. It reflects an elevated content of clay admixture in the protolith. The high REE concentrations (ΣREE = 200–213 ppm, Table 2) compared to NASC is typical for the fine-grained fractions (Taylor and McLennan 1985). It is explained as a result of the high contribution of clays in fine-grained fractions of the protolith.

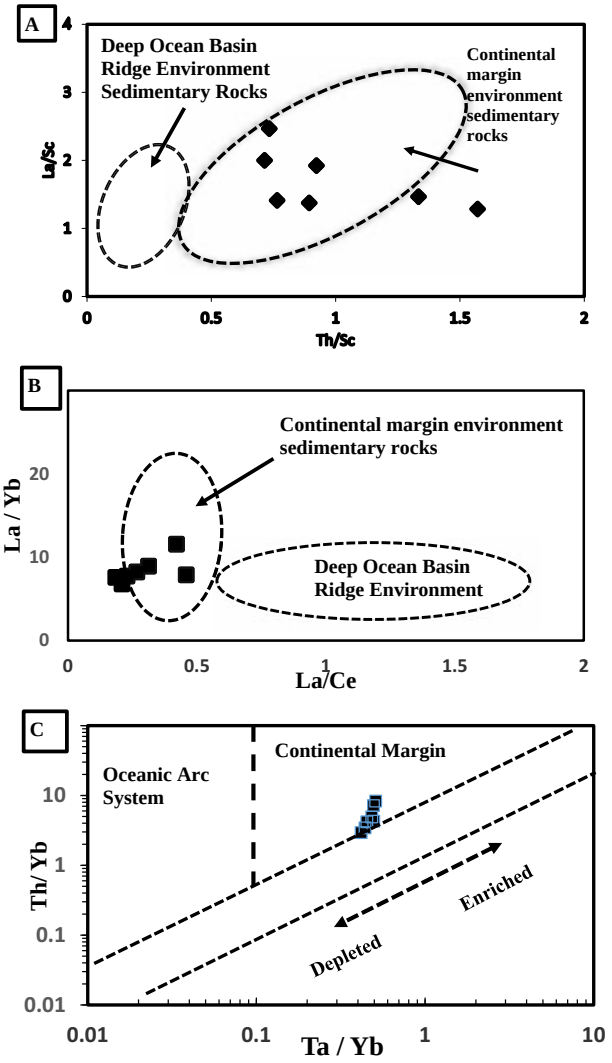

Fig. 11 Geochemical classification of Mlay Lexaugira phyllites: **A** La/Sc versus Th/Sc; **b** La/Yb versus La/Ce after Méres (2005); **C** Th/Yb versus Ta/Yb after Cluzel et al. (2001)

4.3 Mineral chemistry

White micas are generally muscovite with a similar composition in the samples, with Si content ranging from 4.47 to 7.08 ions per formula unit (p.f.u.). The Mg# [(Mg/$Mg^{+}Fe^{+2}$)] is 1, and it is similar to the average ratio observed in the investigated chamosite. Na and Ti contents are below the detection limit. The K content in muscovite ranges from almost zero to 1.38 wt%, while that of Ca is < 0.7 wt%. White micas in all samples are close to the ideal muscovite formula, indicating the presence of the ferri-muscovite component (Table S2). The chlorite of Sirginil phyllite is the

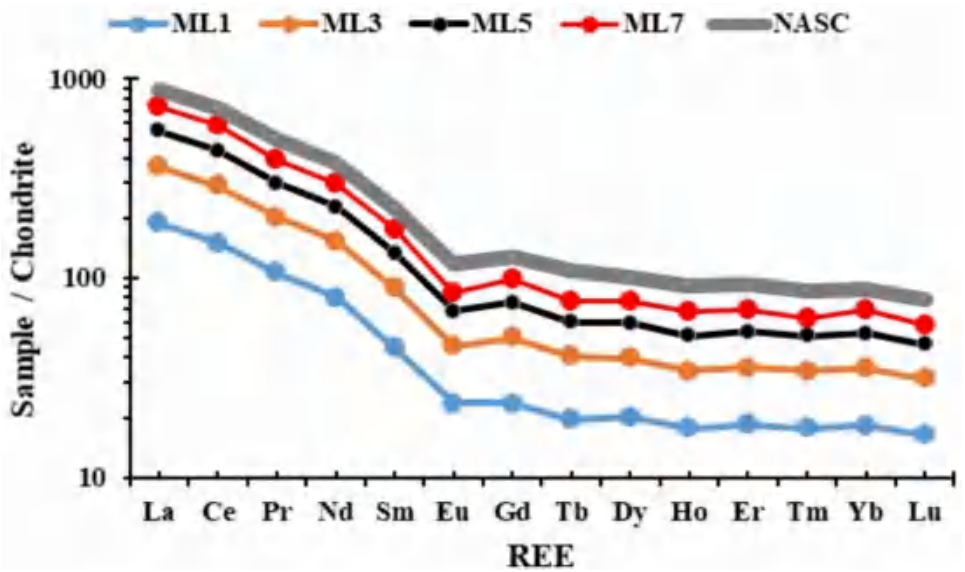

Fig. 12 Chondrite normalized REE pattern of the studied samples, normalized values after Palme (1988)

Table 2 REE concentration in Sirginil phyllite samples (chondrite normalized value according to O'Neill et al. 1998); North American shale composition (NASC) values after Gromet et al. (1984)

REE (ppm)	Chondrite	NASC	ML1	ML3	ML5	ML7
La	0.24	39.00	45.60	42.00	44.30	41.30
Ce	0.61	76.00	92.30	86.80	88.40	90.00
Pr	0.10	10.30	10.71	9.61	9.87	9.10
Nd	0.47	37.00	37.80	34.30	35.60	33.98
Sm	0.15	7.00	6.70	6.70	6.80	6.40
Eu	0.06	2.00	1.41	1.32	1.37	1.02
Gd	0.21	6.10	4.97	5.63	5.30	4.90
Tb	0.04	1.30	0.78	0.84	0.79	0.68
Dy	0.25	6.00	5.05	4.92	4.98	4.40
Ho	0.06	1.40	1.06	1.00	1.02	0.97
Er	0.17	4.00	3.14	2.91	3.12	2.75
Tm	0.03	0.58	0.46	0.43	0.45	0.31
Yb	0.17	3.40	3.10	2.90	3.00	2.71
Lu	0.03	0.60	0.49	0.45	0.46	0.35
∑ REE	2.59	194.68	213.57	199.81	204.16	198.87
∑LREE			193.11	179.41	184.97	193.98
∑HREE			20.46	20.40	20.49	23.42
∑LREE/∑HRRE			9.44	8.79	9.03	8.28
$(La/Yb)_n$			10.42	10.26	10.15	10.79
Gd/Yb_n			1.30	1.57	1.43	1.46
Eu/Eu^*			0.17	0.15	0.16	0.17

predominant secondary mineral in all samples, providing the rock's greenish color (Figs. 5A, B). Composition of chlorites, analyzed by SEM, is presented in Table S2. According to Laird (1988), the $(Al)_n/(Al+Mg+Fe)_n$ ratio in chlorite, formed by alteration of argillites, is >0.35, while in chlorite transformed from mafic rocks it is < 0.35. In the chlorite of the studied samples, the $(Al)_n/(Al+Mg+Fe)_n$ ratios are >0.35, indicating that the source of these chlorites is from the alteration of argillites; this can be further supported by the plots in Figs. 7, 8, and 9. The (Al + Q)—Mg-Fe compositional classification diagram of chlorite (Zane and Weiss 1998) in the study area shows that the chlorites belong to iron-rich chlorite composed mainly of trioctahedral chamosite (Fig. 13).

Relatively uniform Fe^{+3} in hematite ranges from 1.2 to 1.6 p.f.u. Plagioclase is almost pure albite, orthoclase, and microcline. In these siliceous rock's laminae, very fine-grained graphite alternates with granular quartz, muscovite,

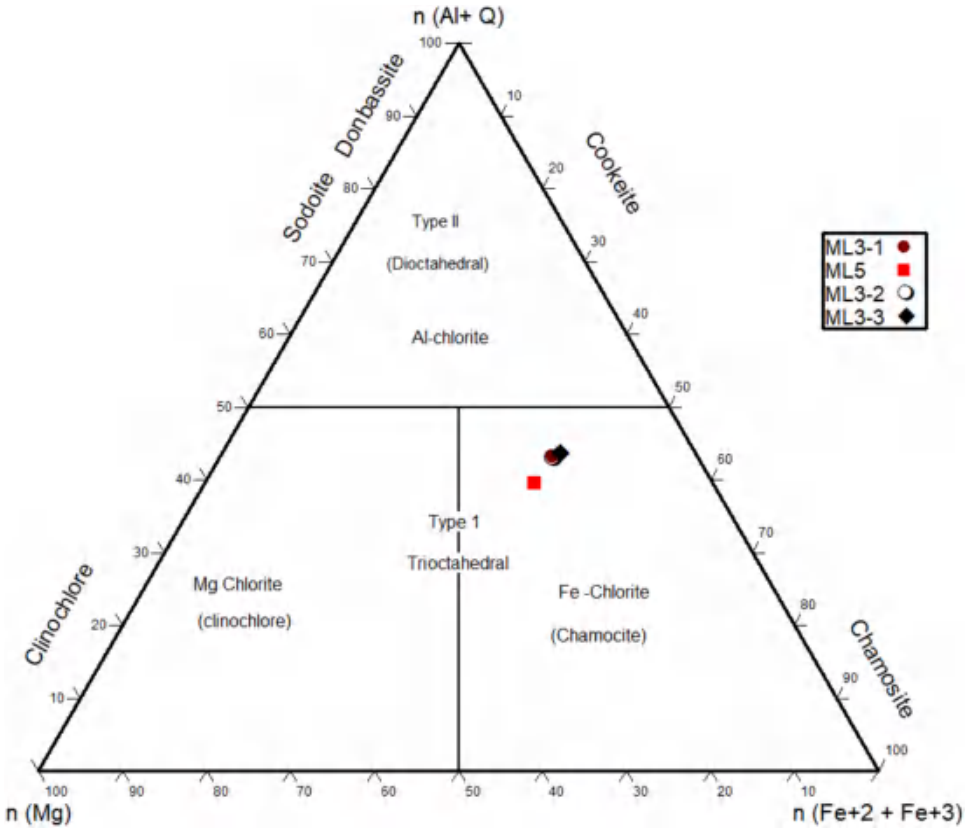

Fig. 13 (Al + Q) –Mg–Fe compositional classification diagram of chlorite in Mlay Lexaugira area according to Zane and Weiss (1998). Note: $Q = 12 - \Sigma(R^{2+} + R^{3+} + R^{4+})_{VI}$ represents structural vacancies

and chlorite (Figs. 5, 6). Allanite, ideally $(Ce,Ca,Y)_2(Al,Fe^{+3})_3(SiO_4)_3(OH)$, was observed in phyllite samples, especially in ML3. To our knowledge, this is the first occurrence of this relatively rare mineral in the studied samples. Figure 5C and the chemical data obtained by few measured ilmenite points (Table S2) show that ilmenite occurs as subhedral to anhedral crystals with sharp edges. Ilmenite intergrows with quartz and muscovite, displaying features indicative of partial dissolution, i.e., its grain boundaries are corroded (Fig. 5 C, G). The ideal chemical formula of ilmenite in the studied samples is $Fe_{0.71}Ti_{0.78}$. Rhodonite with the ideal formula $(Mn_{1.32}Fe^{+3}{}_{0.099}Mg_{0.069}Si_{0.5}O_3)$ is registered as well.

4.4 Chemical alteration, paleoweathering conditions, and provenance

The textural features of the original rocks could have been altered during diagenesis and metamorphism; thus, recognition is hindered. The relative degree of alteration is defined by the chemical index of alteration (CIA = molar proportion $[Al_2O_3/(Al_2O_3 + CaO^* + Na_2O + K_2O)] \times 100$) (Nesbitt and Young 1982). The equation for the chemical index of weathering (CIW) as proposed by Harnois (1988) is like the CIA except that K_2O is not involved in the equation.

The chemical index of alteration (CIA) and the chemical index of weathering (CIW) provide information about the elemental redistribution and amount of weathering in the source region and are therefore frequently utilized to evaluate the severity of alteration and weathering of the source rock (Ismail et al. 2024).

McLennan et al. (1993) and Mongelli et al. (2006) provide the following ranges for both CIA and CIW: values of 50 reflect unweathered or fresh bedrock (no chemical weathering), whereas values close to 100 reflect complete conversion of feldspars to clay minerals (intense chemical weathering). Fedo et al. (1995) also confirmed that when the value of the CIA is as low as ≤ 50, it might reflect cool and/or arid conditions. In the study area, the CIA and the CIW range from 66.39 to 76.38 wt% and 77.43 to 92.39 wt%, with an average value of 74.2 and 88.74 wt%, respectively (Table S1). This is an indication of high to intense weathering under humid conditions.

The index of compositional variability (ICV) (Cox et al. 1995) can be applied to sedimentary rocks to determine their compositional maturity. Immature sedimentary rocks usually show high ICV values (ICV > 1) typical of the first-cycle deposits, indicating a tendency to occur in tectonically active settings. In contrast, compositionally mature sedimentary rocks usually show low ICV values (ICV < 1) typical of

recycled deposits and characteristics of tectonically quiescent or cratonic environments (Cox et al. 1995). The ICV values of the studied samples range between 77 and 100 (mean 82.83) (Table S1), indicating low maturity and first-cycle deposits related to tectonically active settings (Wang et al. 2013; Ofili et al. 2022).

The distribution of some major and trace elements reflects the source area composition; generally, Fe, Mg, Cr, and Ni are related to mafic sources, whereas Al, La, and Nb are typical of felsic sources (Aliyari et al. 2014, Mitwally and Yu 2023). Cr shows high values for some samples of the phyllite suites (Ml1, M3, and ML7) and may be related to heterogeneous source areas characterized by both felsic and mafic features.

Metapelites show low values of Cr/Th (average 6.85), relatively high La/Sc (average 1.70) (Table S1), and strong negative Eu anomaly (average 0.153) (Fig. 12), indicating their origin from an evolved felsic source (Šoster et al. 2020).

Hayashi et al. (1997) proposed that the Al_2O_3/TiO_2 ratios in fine-grained siliciclastic rocks could be directly traced back to the ratios of the corresponding major igneous protoliths. Rocks with an Al_2O_3/TiO_2 ratio >21 are considered to be derived from a felsic source; the ratio of intermediate rocks is between 21 and 8, while rocks of mafic origin have Al_2O_3/TiO_2 ratios of <8. Hayashi et al. (1997) showed similar behavior for the TiO_2/Zr ratio, whereas it decreased from 200 in mafic rocks to 55 in rocks from a felsic source.

The Al_2O_3/TiO_2 ratios (19.66–24. 05; median 22.52) and TiO_2/Zr ratios (35.3–47.09 median 42.70) of the studied metapelitic samples are variable because they derive from felsic to intermediate sources. Using the TiO_2–Al_2O_3 diagram, mafic (basaltic) and felsic (granitic) source rocks were discriminated (Fig. 14); samples were plotted between the basalt + granite and granite + basalt boundaries, suggesting heterogeneous source areas. The A-C + N-K (Al_2O_3–CaO + Na_2O–K_2O) system is useful for evaluating fresh rock compositions and examining their weathering trends because the upper crust is dominated by plagioclase- and K-feldspar–rich rocks and their weathering products, the clay minerals (Nesbitt and Young 1984, 1989). The ternary diagram Al_2O_3–CaO + Na_2O–K_2O by Fedo et al. (1995) was used to ascertain palaeoweathering conditions as well as post-depositional K- metasomatism. From this diagram, trends resulting from the chemical weathering of crystalline bedrock are roughly parallel to the K_2O–Al_2O_3 boundary. The analyzed Sirginil phyllites, plotted in the A–CN–K diagram (Fig. 15), define a linear array that is distinctly different from the expected weathering trend. A straight line through the data intersects the feldspar join at a point representing the fresh composition of potential bedrock. In this case, the bedrock source is dominantly granodiorite to andesite in composition.

The weathering trend as shown in the A–CN–K diagram (Fig. 15) indicates that the analyzed phyllites have undergone post-depositional K metasomatism (i.e., possibly K-metasomatism of illite).

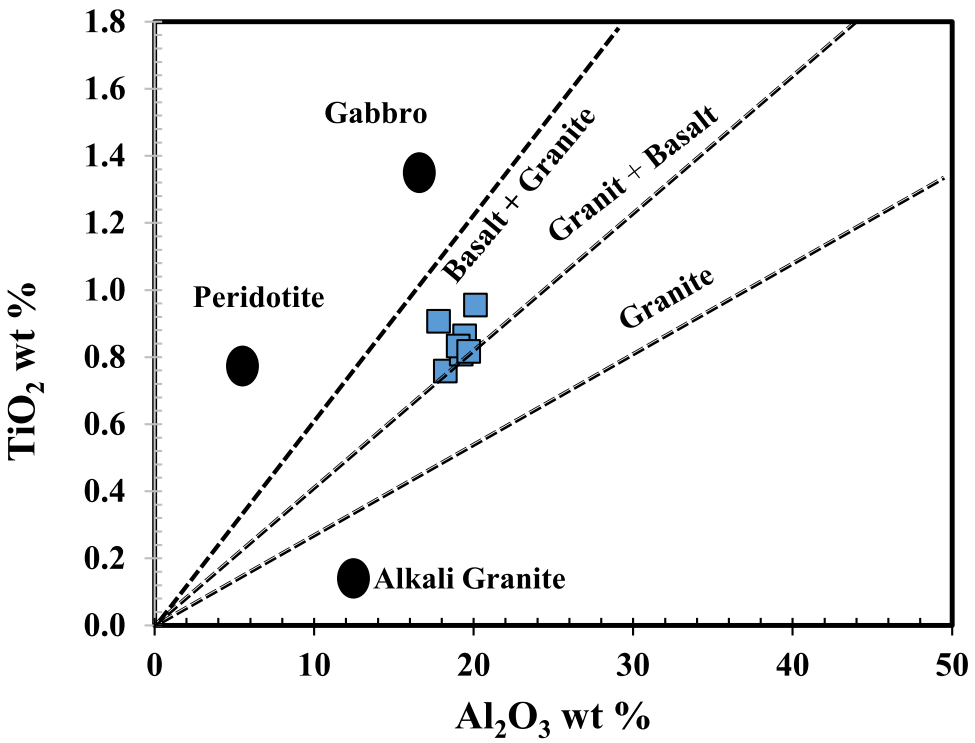

Fig. 14 Plot of TiO_2 versus Al_2O_3 ratios used to determine source rock compositions for the Mlay Lexaugira phyllite samples

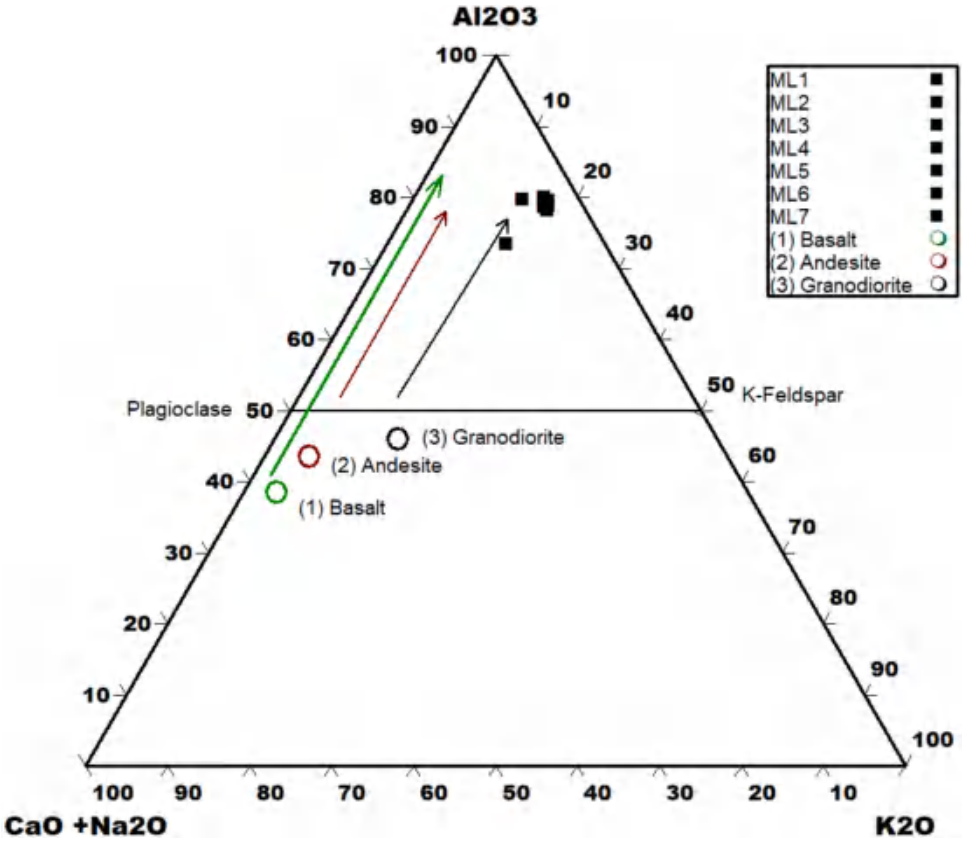

Fig. 15 A–CN–K ternary plot for the Mlay Lexaugira phyllites; pre-metasomatized CIA values can range from ~50 for fresh primary igneous rocks to a maximum of 100 for the most weathered rocks (Fedo et al. 1995); average data of basalt (1), andesite (2), and granodiorite (3) are taken from Méres (2005). The arrows are trends for the weathering of the protolith

The range of intracrustal differentiation is well indicated by ratios La_N/Yb_N and Eu/Eu*(Mclennan et al. 1993). The higher values of La_N/Yb_N (> 10) and values Eu/Eu* in the range of the values 0.15–0.17 indicate that protolith of metamorphosed sedimentary rocks of the Sirginil phyllite group represented the more differentiated crustal material (Fig. 16B).

Based on geochemical data of the Sirginil phyllites and using the La-Th-Sc ternary diagram proposed by Bhatia and Crook (1986) and Eu/Eu* vs. Lan/Yb_n by Méres (2005), most of the samples are plots in the field of the continental margin (Fig. 16A, B). This assessment coincides with the results obtained from the plots La/Sc vs. Th/Sc, La/Yb vs. La/Ce and Th/Yb vs. Ta/Yb. Cluzel et al. (2001) in Fig. 11 support deposition in the continental margin.

The differentiation between mafic and felsic provenance, together with the estimation of the degree of sorting and accumulation of heavy minerals, can be achieved by the ratios of compatible and incompatible element pairs such as Zr/Sc and Th/Sc (McLennan et al. 1993). Zirconium is mainly bound in zircon and serves as a proxy for the degree of sorting, whereas Th is rather concentrated in sediments derived from highly developed magmatic protoliths (Šoster et al. 2020). Th and Zr elements are compared with Sc, which generally retains the signature of the parent rock. In addition, the Th/Sc ratio commonly reflects the average composition of the source rocks. Scandium and Th are transferred quantitatively from source to sediment; hence, the ratio is used to deduce the composition of the source rock (McLennan et al. 1993). The studied phyllite samples show a simple positive correlation between these ratios. The Th/Sc ratios are (0.71–1.57; median 0.99) (Table S1) and have a characteristic of origin from predominantly felsic igneous source, while Zr/Sc ratios (11.47–14.50; median 13.49) indicate only a minor degree of sorting and zircon addition in all samples (Fig. 16C).

5 Conclusions

The protoliths of the Sirginil Group were greywackes and shales, deposited in a relatively oxidized environment. Minor organic matter fragments were syngenetically deposited as the occurrence of graphite indicates.

Geochemical indices such as CIA, CIA', and ICV provide useful insights into the maturity of the sedimentary protolith. The CIA and CIW indices indicate a high degree of chemical weathering or a relatively immature source area. Similarly, ICV indicates low maturity for the studied samples and, thus, the first-cycle deposition related to the continental margin setting.

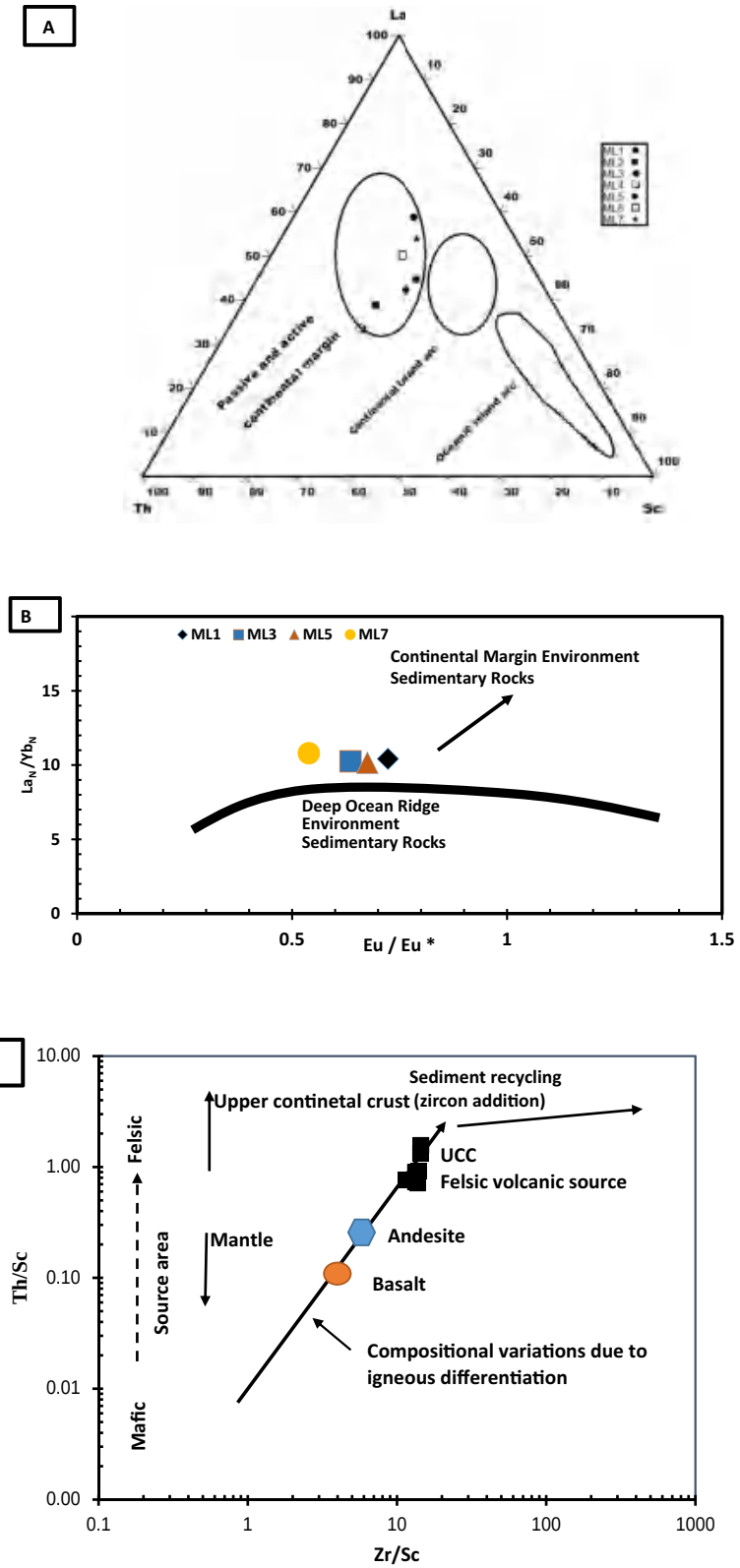

Fig. 16 **A** Plot of the Mlay Lexaugira phyllite samples of the Sirginil Group in the tectonic discrimination plots La–Sc–Th after Bhatia and Crook (1986) and **B** Eu/Eu* versus Lan/Ybn after Méres (2005). **C** Discrimination plot Th/Sc versus Zr/Sc after McLennan et al. (1993) establishes the degree of sorting, recycling, and upper crustal input

The REE composition and fractionated REE pattern, coupled with prominent negative Eu anomaly and low Th/Sc ratios along the La/Sc versus Th/Sc, La/Yb versus La/Ce and Th/Yb versus Ta/Yb plots, indicate a continental margin environment as the provenance for these metasedimentary units.

Acknowledgements The authors thank Vaya Xanthopoulou, Laboratory of Electron Microscopy and Microanalysis, Faculty of Natural Sciences, University of Patras, for conducting the XRD, XRF, and SEM analysis.

Author contributions T. A. Mirza: writing—original draft, resources, methodology, funding acquisition, conceptualization; Abdalla: methodology, investigation, data curation; Sophia Tsiotou methodology, investigation, data curation; Stavros Kalaitzidis: methodology, validation, resources, writing—review & editing.

Funding There was no funding for this manuscript.

Declarations

Conflict of interest The authors declare that they have no known competing financial interests or personal relationships that could have appeared to influence the work reported in this paper. On behalf of all authors, the corresponding author states that there is no conflict of interests.

References

Agard P, OmranI J, Jolivet L, Mouthereau F (2005) Convergence history across Zagros (Iran): Constraints from collisional and earlier deformation. Int J Earth Sci 94:401–419. https://doi.org/10.1007/s00531-005-0481-4

Alavi M (1994) Tectonics of the Zagros orogenic belt of Iran: New data and interpretations. Tectonophysics 229(3–4):211–238. https://doi.org/10.1016/0040-1951(94)90030-2

Aliyari F, Rastad E, Goldfarb RJ, Sharif JA (2014) Geochemistry of hydrothermal alteration at the Qolqoleh gold deposit, northern Sanandaj-Sirjan metamorphic belt, northwestern Iran: vectors to high-grade ore bodies. J Geochem Explor 140:111–125. https://doi.org/10.1016/j.gexplo.2014.01.007

Al-Kadhimi JA, M Sissakian VK, Fattah, AS Deikran DB (1996) Tectonic map of Iraq (scale 1:1000 000, 2nd ed). Baghdad, Iraq, 1–38.

Al-Qayim B, Omer A, Koyi H (2012) Tectonostratigraphic overview of the Zagros suture zone, Kurdistan Region, northeast Iraq. GeoArabia 17(4):109–156. https://doi.org/10.2113/geoarabia1704109

Awadh SM, Kettanah Y (2008) Petrology, geochemistry and tectonical environment of the Shalair metamorphic rock group and katar rash volcanic group, Shalair Vally area, northeastern Iraq. Iraqi J Sci 49(1):149–158

Bhatia MR, Crook KAW (1986) Trace element characteristics of graywackes and tectonic setting discrimination of sedimentary basins. Contrib Mineral Petrol 92(2):181–193. https://doi.org/10.1007/BF00375292

Bock B, McLennan SM, Hanson GN (1998) Geochemistry and provenance of the middle Ordovician Austin glen member (Normanskill formation) and the Taconian orogeny in new England. Sedimentology 45(4):635–655. https://doi.org/10.1046/j.1365-3091.1998.00168.x

Bokanda EE, Fralick P, Ekomane E, Bisse SB, Tata CN, Ashukem EN, Belinga BC (2021) Geochemical constraints on the provenance, paleoweathering and maturity of the Mamfe black shales. West Africa J Afr Earth Sci 175:104078. https://doi.org/10.1016/j.jafrearsci.2020.104078

Buday T (1980) The regional geology of Iraq: Stratigraphy and paleogeography (Vol. 1). State Organization for Minerals, Directorate General for Geological Survey

Cambel B, Khun M (1983) Geochemical characteristics of black shales from ore bearing complex of the Malé Karpaty. Geol Carpath 34:15–44

Cambel B, Khun M (1985) Rare earth elements in metamorphosed black shales of the Malé Karpaty Mts. Geologický Zborník 36:3–16

Cambelb PE (1985) Biostratigraphic evaluation of metasediments in the Malé Karpaty Mts. region. Geologický Zborník 36:683–700

Cluzel D, Aitchison JC, Picard C (2001) Tectonic accretion and underplating of mafic terranes in the Late Eocene intraoceanic fore-arc of New Caledonia (Southwest Pacific): Geodynamic implications. Tectonophysics 340(1–2):23–59. https://doi.org/10.1016/S0040-1951(01)00148-2

Condie KC (1993) Chemical composition and evolution of the upper continental crust: Contrasting results from surface samples and shales. Chem Geol 104(1–4):1–37. https://doi.org/10.1016/0009-2541(93)90140-E

Cox R, Lowe DR, Cullers RL (1995) The influence of sediment recycling and basement composition on evolution of mudrock chemistry in the southwestern United States. Geochim Cosmochim Acta 59(14):2919–2940. https://doi.org/10.1016/0016-7037(95)00185-9

Cullers RL (1995) The controls on the major- and trace-element evolution of shales, siltstones and sandstones of Ordovician to tertiary age in the Wet Mountains region, Colorado, USA. Chem Geol 123(1–4):107–131. https://doi.org/10.1016/0009-2541(95)00050-V

Fedo CM, Wayne Nesbitt H, Young GM (1995) Unraveling the effects of potassium metasomatism in sedimentary rocks and paleosols, with implications for paleoweathering conditions and provenance. Geology 23(10):921. https://doi.org/10.1130/0091-7613(1995)023%3c0921:uteopm%3e2.3.co;2

Garver J, Royce P, Smick T (1996) Chromium and nickel in shale of the taconic foreland: a case study for the provenance of fine-grained sediments with an ultramafic source. SEPM J Sediment Res 66(1):100–106. https://doi.org/10.1306/d42682c5-2b26-11d7-8648000102c1865d

Gromet LP, Haskin LA, Korotev RL, Dymek RF (1984) The "north American shale composite": Its compilation, major and trace element characteristics. Geochim Cosmochim Acta 48(12):2469–2482. https://doi.org/10.1016/0016-7037(84)90298-9

Harnois L (1988) The CIW index: a new chemical index of weathering. Sed Geol 55:319–322. https://doi.org/10.1016/0037-0738(88)90137-6

Hayashi KI, Fujisawa H, Holland HD, Ohmoto H (1997) Geochemistry of ~1.9 Ga sedimentary rocks from Northeastern Labrador Canada. Geochim Cosmochim Acta 61(19):4115–4137. https://doi.org/10.1016/S0016-7037(97)00214-7

Heiri O, Lotter AF, Lemcke G (2001) Loss on ignition as a method for estimating organic and carbonate content in sediments: reproducibility and comparability of results. J Paleolimnol 25(1):101–110. https://doi.org/10.1023/A:1008119611481

Herron MM (1988) Geochemical classification of terrigenous sands and shales from core or log data. SEPM J Sediment Res 58:820–829. https://doi.org/10.1306/212f8e77-2b24-11d7-8648000102c1865d

Ismail SA, Ali SA, Nutman AP, Bennett VC, Jones BG (2017) The Pushtashan juvenile supra subduction zone assemblage of Kurdistan (Northeastern Iraq): A Cretaceous (Cenomanian) Neo-Tethys missing link. Geosci Front 8(5):1073–1087. https://doi.org/10.1016/j.gsf.2016.11.002

Ismail I, Ali A, Jassim S (2024) Some geomorphological implications of chemical weathering in sequences of sedimentary rocks in the

Kirkuk structure. Iraqi Geol J 57:293–303. https://doi.org/10.46717/igj.57.1c.19ms-2024-3-31
Ivan P, Méres Š, Putiš M, Kohút M (2001) Early Paleozoic metabasalts and metasedimentary rocks from the Malé Karpaty Mts. (Western Carpathians): Evidence for rift basin and ancient oceanic crust. Geol Carpath 52:67–78
Jassim SZ, Goff JC (2006) Geology of Iraq: Dolin. Brno, Czech Republic, Prague and Moravian Museum, p 5
Kwankam FN, Ekoko Eric B, Adama A, Salomon Bertrant B, Njeck Rexon Junior A, Shannon Ngwakfu N, Fidelis Esue M, Hewett Ekumeli M, Maureen Ntube N, Agyingi MC (2023) Geochemical characterisation of clastic sediments in kompina (N'kapa formation, NW Douala basin, west Cameroon): Implication for provenance, paleoweathering and sediment maturity. Heliyon 9(5):e16034. https://doi.org/10.1016/j.heliyon.2023.e16034
Laird J (1988) Chlorites, metamorphic petrology. Rev Mineral Geochem 19:405–453
Ma'ala K (2008) Geological map of the Sulaimaniya Quadrangle. sheet N1–38–3, scale 1: 20000, GEOSURV
MacDonald GA, Katsura T (1964) Chemical composition of Hawaiian Lavas. J Petrol 5(1):82–133. https://doi.org/10.1093/petrology/5.1.82
McLennan SM, Hemming S, McDaniel DK, Hanson GN (1993) Geochemical approaches to sedimentation, provenance, and tectonics. Processes controlling the composition of clastic sediments. Geological Society of America, pp 21–40. https://doi.org/10.1130/spe284-p21
McLennan SM (2018) Rare earth elements in sedimentary rocks: Influence of provenance and sedimentary processes. Geochemistry and Mineralogy of Rare Earth Elements. De Gruyter, pp 169–200. https://doi.org/10.1515/9781501509032-010
Méres Š (2005) Major, trace element and REE geochemistry of metamorphosed sedimentary rocks from the Malé Karpaty Mts. (Western Carpathians, Slovak Republic): Implications for sedimentary and metamorphic processes. Slovak Geological Magazine, 11(2–3):107–122.
Mirza TA, Kalaitzidis SP, Mohammed SH, Rashid SG, Petrou X (2017) Geochemistry and genesis of sulphide ore deposits in Sharosh Village, Qandil Series, Kurdistan Region, NE Iraq. Arabian J Geosci 10:1–19. https://doi.org/10.1007/s12517-017-3210-y
Mirza TA, Kalaitzidis SP, Fatah SS, Tsiotou S (2021) Petrographic and geochemical features of Gimo marble, Gole area, Kurdistan Region, Iraq: Constraints on its protolith's origin and depositional environment. Earth Sci Res J 25(3):285–295. https://doi.org/10.15446/esrj.v25n3.88686
Mirza TA, Salih NM, Delpomdor FRA, Kalaitzidis SP, Rashid SG (2022) Formation of quartz veins within Serginil Phyllite group-Penjween area, Iraqi Kurdistan region: insights from geochemical and fluid inclusion data. Arab J Geosci 15(9):887. https://doi.org/10.1007/s12517-022-10143-0
Mohammed Ali Mitwally E, Yu BS (2023) Geochemical studies and resource potential of magnetite in Taiwanese beach sands and related source rocks: implications for geochemical fingerprinting of ore minerals. Ore Geol Rev 162:105649. https://doi.org/10.1016/j.oregeorev.2023.105649
Mongelli G, Critelli S, Perri F, Sonnino M, Perrone V (2006) Sedimentary recycling, provenance and paleoweathering from chemistry and mineralogy of Mesozoic continental redbed mudrocks, Peloritani mountains, southern Italy. Geochem J 40(2):197–209. https://doi.org/10.2343/geochemj.40.197
Mustafa Mirza TA, Kalaitzidis SP (2023) Petrographical and geochemical features of sulfide mineralization in the Walash Group, Gallala Area, Kurdistan Region of Iraq. Iraqi Geol J 56:19–36. https://doi.org/10.46717/igj.56.2E.2ms-2023-11-7
Nesbitt HW, Young GM (1982) Early Proterozoic climates and plate motions inferred from major element chemistry of lutites. Nature 299:715–717. https://doi.org/10.1038/299715a0
Nesbitt HW, Young GM (1984) Prediction of some weathering trends of plutonic and volcanic rocks based on thermodynamic and kinetic considerations. Geochim Cosmochim Acta 48(7):1523–1534. https://doi.org/10.1016/0016-7037(84)90408-3
Nesbitt HW, Young GM (1989) Formation and diagenesis of weathering profiles. J Geol 97(2):129–147. https://doi.org/10.1086/629290
Ofili S, Soesoo A, Panova EG, Hints R, Hade S, Ainsaar L (2022) Geochemical reconstruction of the provenance, tectonic setting and paleoweathering of lower Paleozoic black shales from northern Europe. Minerals 12(5):602. https://doi.org/10.3390/min12050602
O'Neill HSC, Canil D, Rubie DC (1998) Oxide-metal equilibria to 2500 °C and 25 GPa: implications for core formation and the light component in the Earth's core. J Geophys Res Solid Earth 103(B6):12239–12260. https://doi.org/10.1029/97jb02601
Palme H (1988) Chemical abundances in meteorites. Cosmic Chemistry. Springer, Berlin Heidelberg, Springer, pp 28–51
Qaradaghi J, Mirza TA (2023) Peperites: insight into the submarine eruptions within Walash Volcano sedimentary Group, Mawat Area, Iraqi Kurdistan Region. ARO Sci J Koya Uni 11(2):157–177. https://doi.org/10.14500/aro.11363
Rana H, Thomas H, Soni A, Shukla S (2023) Petrochemistry of phyllites from Patharkhola, Lesser Kumaun Himalaya with reference to tectonic implications. Earth Planet Sci 2(2):1–9. https://doi.org/10.36956/eps.v2i2.842
Sharland P, Archer R, Casey D, Davies R, Hall S, Heward A, Horbury A, Simmons M (2001) Gulf Petrolink. Arab Plate Sequ Stratigr Geo 2:371
Silwal BR, Gyawali BR, Yoshida K (2024) Geochemical and mineralogical analysis of low-grade metamorphic rocks and their response to shallow landslide occurrence in Central Nepal. Geoenviron Disasters 11(1):37. https://doi.org/10.1186/s40677-024-00301-9
Šoster A, Zavašnik J, O'Sullivan P, Herlec U, Krajnc BP, Palinkaš L, Zupančič N, Dolenec M (2020) Geochemistry of bashibos-bajrambos metasedimentary unit, serbo-macedonian massif, North Macedonia: Implications for age, provenance and tectonic setting. Geochemistry 80(4):125664. https://doi.org/10.1016/j.chemer.2020.125664
Taylor, S R, Mclennan SM (1985) The continental crust: its composition and evolution. Blackwell Scientfic Publications. pp333
Wang ZM, Han CM, Su BX, Sakyi PA, Malaviarachchi SP, Ao SJ, Wang LJ (2013) The metasedimentary rocks from the eastern margin of the Tarim Craton: petrology, geochemistry, zircon U-Pb dating, Hf isotopes and tectonic implications. Lithos 179:120–136. https://doi.org/10.1016/j.lithos.2013.08.01
Wentworth CK (1922) A scale of grade and class terms for clastic sediments. J Geol 30(5):377–392. https://doi.org/10.1086/622910
Wignall PB, Twitchett RJ (1996) Oceanic anoxia and the end Permian mass extinction. Science 272(5265):1155–1158. https://doi.org/10.1126/science.272.5265.1155
WRAFTER' JP, Graham JR (1989) Short paper: ophiolitic detritus in the ordovician sediments of South Mayo. Ireland. J Geol Soc 146(2):213–215. https://doi.org/10.1144/gsjgs.146.2.0213
Zane A, Weiss Z (1998) A procedure for classifying rock-forming chlorites based on microprobe data; Una procedura per la classificazione delle cloriti sulla base di dati microchimici. Atti della Accademia Nazionale dei Lincei. Rend Sci Fisiche e Naturali 9:51–56

Springer Nature or its licensor (e.g. a society or other partner) holds exclusive rights to this article under a publishing agreement with the author(s) or other rightsholder(s); author self-archiving of the accepted manuscript version of this article is solely governed by the terms of such publishing agreement and applicable law.